Published in final edited form as:
J Magn Reson Imaging. 2008 May ; 27(5): 1175–1180. doi:10.1002/jmri.21337.

Positive Contrast MR-Lymphography Using Inversion Recovery With ON-Resonant Water Suppression (IRON)

Grigorios Korosoglou, MD[1,2], **Lijun Tang, MD**[2], **Dorota Kedziorek, MD**[2], **Kenyatta Cosby, MD**[2], **Wesley D. Gilson, PhD**[2], **Evert-Jan Vonken, MD, PhD**[2], **Michael Schär, PhD**[2,3], **David Sosnovik, MD**[4], **Dara L. Kraitchman, VMD, PhD**[2], **Robert G. Weiss, MD**[2,5], **Ralf Weissleder, MD, PhD**[4], and **Matthias Stuber, PhD**[2,*]

[1]University of Heidelberg, Department of Cardiology, Heidelberg, Germany. [2]Russell H. Morgan Department of Radiology and Radiological Science, Johns Hopkins University School of Medicine, Baltimore, Maryland. [3]Philips Medical Systems, Cleveland, Ohio. [4]Center for Molecular Imaging Research, Massachusetts General Hospital, Harvard Medical School, Boston, Massachusetts. [5]Cardiology Division, Department of Medicine, Johns Hopkins University School of Medicine, Baltimore, Maryland.

Abstract

Purpose—To investigate the utility of inversion recovery with ON-resonant water suppression (IRON) to create positive signal in normal lymph nodes after injection of super-paramagnetic nanoparticles.

Materials and Methods—Experiments were conducted on six rabbits, which received a single bolus injection of 80 μmol Fe/kg monocrystalline iron oxide nanoparticle (MION-47). Magnetic resonance imaging (MRI) was performed at baseline, 1 day, and 3 days after MION-47 injection using conventional T_1- and T_2*-weighted sequences and IRON. Contrast-to-noise ratios (CNR) were measured in blood and in paraaortic lymph nodes.

Results—On T_2*-weighted images, as expected, signal attenuation was observed in areas of paraaortic lymph nodes after MION-47 injection. However, using IRON the paraaortic lymph nodes exhibited very high contrast enhancement, which remained 3 days after injection. CNR with IRON was 2.2 ± 0.8 at baseline, increased markedly 1 day after injection (23.5 ± 5.4, $P < 0.01$ vs. baseline), and remained high after 3 days (21.8 ± 5.7, *$P < 0.01$ vs. baseline). CNR was also high in blood 1 day after injection (42.7 ± 7.2 vs. 1.8 ± 0.7 at baseline, $P < 0.01$) but approached baseline after 3 days (1.9 ± 1.4, P = NS vs. baseline).

Conclusion—IRON in conjunction with superparamagnetic nanoparticles can be used to perform 'positive contrast' MR-lymphography, particularly 3 days after injection of the contrast agent, when signal is no longer visible within blood vessels. The proposed method may have potential as an adjunct for nodal staging in cancer screening.

Keywords

inversion recovery with ON-resonant water suppression (IRON); off-resonance imaging; monocrystalline iron oxide nanoparticle (MION-47); magnetic resonance lymphography

*Address reprint requests to: M.S., PhD, Johns Hopkins University Medical School, Russell H. Morgan Department of Radiology and Radiological Science, JHOC 4223, 601 North Caroline St., Baltimore, MD 21287. E-mail: mstuber@mri.jhu.edu.

Contrast-enhanced magnetic resonance (MR)-lymphography is a potential noninvasive method for the evaluation of the lymphatic system and in particular for nodal staging (1–10). The most widely evaluated intravenous contrast agents for MR-lymphography are superparamagnetic nanoparticles, which accumulate slowly in macrophages of the lymph nodes and show maximum lymphographic effects 24 hours after injection. Several experimental (1–5) and clinical studies (6–10) have demonstrated the accuracy for lymph node evaluation after the administration of superparamagnetic nanoparticles for the evaluation of pelvic, abdominal, thoracic, head, and neck tumors.

Conventional strategies for MR-lymphography take advantage of magnetic susceptibility artifacts, creating negative signal in normal lymph nodes, which accumulate superparamagnetic nanoparticles, while the signal in metastatic lymph nodes remains unchanged (1–10). However, negative signal may arise from many other sources such as the absence of tissue, motion, or calcifications. This may hamper the ability of conventional methods to discriminate between normal lymph nodes with low signal and other sources of signal loss (4,9).

Recently, spectrally selective radiofrequency (RF) pulses have been reported to create positive signal using superparamagnetic materials (11–15). This positive signal is a result of off-resonance effects in areas of superparamagnetic particles. Inversion recovery with ON-resonant water suppression (IRON) is a new approach which creates positive signal in areas of superparamagnetic nanoparticles and simultaneously suppresses signal from tissues which do not contain iron (16). The purpose of the present study was to test the hypothesis whether IRON can create positive signal in normal lymph nodes after the systemic administration of superparamagnetic nanoparticles. This hypothesis was tested in a rabbit model at 3T.

MATERIALS AND METHODS

Animals and Imaging Agent

The studies were approved by the Institutional Animal Care and Use Committee. Experiments were conducted on six male rabbits (2.5–3.2 kg). The animals were sedated with acepromazine (1 mg/kg I.M.) and ketamine (40 mg/kg I.M.), and general anesthesia was maintained with intravenous thiopental. Monocrystalline iron oxide nanoparticle (MION)-47 was administrated as a single bolus injection of 80 μmol Fe/kg in all six rabbits. The physical, chemical, and MR properties of MION-47 are described elsewhere (17,18).

MR Imaging

All animals were imaged in the supine position using a commercial 3T whole body scanner (Achieva, Philips Medical Systems, Best, the Netherlands) and a 4-element human carotid receiver coil (Pathway MRI, Seattle, WA). Imaging was performed at baseline and 1 day and 3 days after MION-47 injection.

Conventional T_1- and T_2*-Weighted Imaging—For T_1-weighted imaging, 3D gradient-echo images of the abdomen were obtained using the following parameters: TR/TE = 25/2.7 msec, 20° excitation angle, 200 × 100 mm field of view (FOV), partial echo, bandwidth = 217 Hz/pixel, RF spoiling, and a 400 × 200 matrix. A 5.0-cm thick 3D volume was scanned with 50 z-encoding steps (0.5 × 0.5 × 1 mm^3 acquired resolution). Scanning time was 3 minutes. For T_2*-weighted imaging TR/TE was modified to 100/12 msec and the excitation angle was changed to 6°. All other parameters were kept identical to those of the T_1-weighted imaging. The mean size of the abdominal lymph nodes was measured on coronal T_1-weighted images and was expressed as cranio-caudal and left-right diameters.

Inversion Recovery With ON-Resonant Water Suppression (IRON)

Theoretical Background of IRON: The local external field-shift of a nondiamagnetic spherical particle exposed to the static magnetic field (B0) can be described as:

$$\Delta B_{External}(\mathbf{r},\Theta)\sim(\Delta K^{*}a^{3}/3^{*}\mathbf{r}^{3})^{*}(3^{*}\cos^{2}(\Theta)-1)^{*}\mathbf{B}_{0}. \quad (1)$$

In this equation ΔK is the difference in susceptibility between the particle and its surroundings, *r* refers to the distance from the particle, *a* refers to its radius and Θ represents the angle between *r* and B_0. External to the particle, the frequency shift is $\Delta\omega_{External} = \gamma\Delta B_{External}$. The concept of IRON imaging comprises the use of a spectrally selective saturation prepulse on-resonance (ω_0) with the bandwidth of BW_{IRON}, in order to suppress the signal originating from on-resonant protons (Fig. 1a). This saturation pulse does not affect off-resonant protons in areas of superparamagnetic nanoparticles (Fig. 1b). Therefore, signal enhancement adjacent to these particles can be generated while the on-resonant background appears signal-attenuated (Fig. 1c). Fat saturation can be obtained by adding a fat suppression prepulse, as shown in Fig. 1a,b.

IRON Imaging: IRON was combined with gradient-echo and black-blood fast-spin-echo imaging. For all sequences an IRON prepulse with $BW_{IRON}$of 100 Hz, a duration of τ = 50 msec, and an excitation angle a_{IRON} of 100° was used. The preceding frequency selective prepulse used for fat saturation had a frequency offset of −480 Hz, a duration of 10 msec, and an excitation angle of 105°. Typical imaging parameters for the 3D gradient-echo imaging were: TR/TE = 3.9/1.54 msec, 15° excitation angle, 140 × 112 mm FOV, partial echo, bandwidth = 642 Hz/pixel, RF spoiling, and a 288 × 220 matrix. A 5.0 cm thick 3D volume was scanned with 25 z-encoding steps (0.49 × 0.51 × 2 mm^3 acquired resolution). Scanning time was 3 minutes. For 3D black-blood fast-spin-echo imaging, the vector electrocardiogram (VCG) was used for R-wave triggering and the black blood dual-inversion delay was set at 370 msec. Typical parameters were: TR/TE = 857/8.2 msec, 90° excitation angle, 100 × 80 mm FOV, bandwidth = 248 Hz/pixel and a 288 × 288 matrix. A 1.4–2.0-cm thick 3D volume was scanned with 7–10 z-encoding steps (0.35 × 0.27 × 2 mm^3 acquired resolution). Scanning time was 8.5–12 minutes.

Image Analysis

Quantitative analysis was performed by one of the authors (G.K.) using the “soap bubble” tool (19). Soap bubble is a software tool that was previously developed in order to facilitate the visualization and quantitative comparison of 3D volumetric data sets. In its present implementation the soap bubble tool enables the analysis of frequently explored quantitative parameters such as signal-to-noise ratio (SNR) and contrast-to-noise ratio (CNR). CNR was quantified on IRON images, at baseline, on day 1, and on day 3, using original, non-reformatted datasets. Regions of interest (ROIs) were placed manually on paraaortic lymph nodes and in the abdominal aorta of the rabbits for the measurement of the mean signal (S_{lymph} and S_{blood}, respectively). Similar ROIs were placed in adjacent abdominal muscle and in fat to measure S_{muscle} and S_{fat}, respectively, and also in the air outside of the rabbit to calculate standard deviation of this region as a measure of noise ($\sigma_{background}$). CNR was calculated as:

$$CNR_{lymph} = \left(S_{lymph} - S_{fat}\right)/\sigma_{background} \text{ and} \quad (2)$$

$$CNR_{blood} = (S_{blood} - S_{muscle})/\sigma_{background}. \quad (3)$$

Care was taken to standardize ROI size and placement for better comparison of the imaging sets. The size of the ROIs was 0.32 ± 0.05 cm^2 for ROIs placed in vessels, 0.34 ± 0.04 cm^2 for ROIs placed in lymph nodes, 0.37 ± 0.05 cm^2 for ROIs placed in fat, 0.33 ± 0.05 cm^2 for ROIs placed in the abdominal adjacent muscle, and 8.3 ± 1.1 cm^2 for ROIs placed in the background.

Isolation of Abdominal Lymph Nodes and Histopathologic Examination

After MR imaging the rabbits were sacrificed with an overdose of thiopental and the abdominal lymph nodes were isolated and fixed with 4% paraformaldehyde. The lymph nodes were then frozen and 10-μm thick sections were obtained using a cryostat for histological analysis. Tissue sections were stained with Prussian blue to detect iron oxide particles and counterstained with nuclear fast red. In addition, an acid phosphates-estain (Sigma-Aldrich, St. Louis, MO) to detect phagocytic cells was performed on adjacent sections which were then counterstained with Prussian blue as described previously (20).

Statistical Analysis

Data are presented as mean ± one standard deviation. Differences in CNR of the abdominal lymph nodes and in blood between baseline, day 1, and day 3 were compared using a repeated-measures analysis of variance (ANOVA) with Bonferroni post-hoc comparison. Differences were considered statistically significant at $P < 0.05$.

RESULTS

On conventional T_1-weighted images, two major lymph nodes could routinely be identified along the abdominal aorta at the level of the renal arteries in each rabbit (12 abdominal lymph nodes in total, mean size 8.4 ± 1.0 × 9.1 ± 1.1 mm^2) (Fig. 2a, solid arrows). After the administration of MION-47, lymph nodes showed signal void on T_2*-weighted images (Fig. 2b, solid arrow). However, the clear visualization of the lymph nodes was often compromised due to a general lack of signal (Fig. 2b, dotted arrow). Using IRON, fat, muscle, and blood were homogeneously suppressed at baseline (Fig. 2c). One day after injection, paraaortic lymph nodes were clearly visible (Fig. 2d). However, at this timepoint high contrast enhancement was present both in the paraaortic lymph nodes and in the aorta. After 3 days the signal decreased in the vessels but persisted in the lymph nodes (Fig. 2e). The location and morphology of the lymph nodes on MRI corresponded with their in situ localization (Fig. 2f). Corresponding postcontrast fast spin echo IRON images also demonstrated contrast enhancement in paraaortic lymph nodes in coronal (Fig. 3a, solid arrows) and in axial slices (Fig. 3b, solid arrow). Furthermore, in the same animal the lymphatic ducts along the aorta could be clearly visualized with high spatial resolution on coronal (Fig. 3c, hatched arrows) and on axial slices (Fig. 3d, hatched arrows). Note that the abdominal aorta (Fig. 3a,b, arrowheads) and adjacent muscles are signal-attenuated (Fig. 3a,b, dotted arrows) in all IRON images.

Quantitative assessment of IRON images showed that the CNR markedly increased in paraaortic lymph nodes after 24 hours (24.0 ± 5.3 on day 1 vs. 1.4 ± 0.8 at baseline, $*P < 0.01$) and remained high up to 3 days after MION-47 injection (22.3 ± 6.2, $*P < 0.01$ vs. baseline) (Fig. 4). In the aorta, CNR was high 24 hours after MION-47 administration (42.7 ± 7.2 on day 1 vs. 1.8 ± 0.7 at baseline, $\#P < 0.01$) but returned to baseline after 3 days (1.9 ± 1.4, P = NS vs. baseline).

Prussian blue positive staining, representing iron oxide particles, was detected in abdominal lymph nodes of the rabbits (Fig. 5a). Combined acid phosphatase and Prussian blue staining shows colocalization of nodal macrophages (stained red) and accumulated iron (Fig. 5b).

DISCUSSION

This is to our knowledge the first report on 'positive contrast' MR-lymphography using (MION)-47 as an imaging agent. Using IRON, positive signal was created in the areas of superparamagnetic nanoparticles, which accumulated in functional lymphatic tissue. One day after MION-47 injection, contrast enhancement was present both intravascular and in the lymph nodes of the rabbits. On day 3, contrast enhancement was present only in the lymph nodes, while blood and adjacent muscles displayed homogeneously signal suppressed. The potential of this method to differentiate between functional and metastatic lymphatic tissue remains to be elucidated in further studies.

Conventional 'negative contrast' techniques for MR-lymphography are based on local changes of T_2 and T_2*-relaxation rates caused by superparamagnetic nanoparticles (1–10). These changes create susceptibility artifacts, which can be visualized as negative signal in normal lymph nodes using T_2*-weighted imaging, while metastatic lymph nodes remain unchanged. However, a fundamental drawback of 'negative contrast' techniques is that low signal in normal lymph nodes cannot be distinguished from other sources of signal voids due to absence of tissue, motion, or calcifications. Furthermore, 'negative contrast' techniques suffer from partial-volume effects, where the ability to detect a void depends on spatial resolution (13). Particularly when small receiver coils with a small volume of sensitivity are used, the intensity variation across the image may further hamper the accurate identification of negative signal due to susceptibility effects (13). In addition, it should be noted that TE is longer in T_2*-weighted sequences compared to both T_1-weighted and IRON sequences. For this reason, T_2*-weighted images may not only be more sensitive to motion artifacts but a reduced SNR may be another impediment. In agreement with these theoretical concerns the negative signal in the abdominal lymph nodes could not be readily detected as such on the T_2*-weighted images in our study. This was attributed to other sources of signal void caused by absence of tissue or by respiratory motion at the level of the abdomen. However, it should be noted that the comparison of pre- to post-contrast T_2*-weighted images is very useful for the differentiation of functional versus metastatic lymph nodes and may help to overcome some of the susceptibility- related problems and SNR constrains of T_2*-weighted MR-images.

The results of the present study demonstrate the utility of IRON to create positive signal in small normal lymph nodes after a single bolus administration of superparamagnetic nanoparticles. IRON allowed the clear visualization of small lymph nodes (mean size <10 mm), and quantification analysis revealed high CNR in the abdominal lymph nodes 1 and 3 days after contrast agent administration. In particular, 3 days after injection of the superparamagnetic nanoparticles, IRON facilitated the clear visualization of functional lymphatic tissue, because blood, adjacent muscles, and fat are signal-attenuated at this timepoint. IRON can be combined both with conventional gradient echo and fast spin echo sequences in order to create positive signal originating from off-resonance in the area of superparamagnetic nanoparticles, which accumulate in functional lymph nodes.

The present study provides a proof-of-principle for the utility of IRON as a 'positive contrast' technique for MR-lymphography. Due to the small number of animals ($n = 6$) and lymph nodes ($n = 12$) studied, we did not perform a head-to-head comparison of conventional (T_2*-weighted) versus IRON imaging for the delineation of normal lymph nodes. However, this is the aim of future studies. Furthermore, the potential of IRON to differentiate between normal and metastatic lymph nodes was not evaluated in this study, and IRON was not compared to other techniques, which create positive signal in areas of superparamagnetic materials (11–15). Previous studies have shown that, using T_2*-weighted imaging, susceptibility artifacts in areas of accumulated USPIO in functional lymph nodes may obscure small focal metastases within the same or in neighboring lymph nodes. However, it is anticipated that on IRON images

small focal metastases may also be missed due to the suppression of on resonant protons in tissue that does not contain accumulated superparamagnetic nanoparticles (metastatic tissue). An inherent limitation of IRON is that it is based on frequency selection so that IRON images can be affected by susceptibility interfaces and B_1-inhomogeneity. Thus, unwanted magnetization from regions that are shifted in frequency, such as tissue near the lungs or intestines, could also create positive signal on the images. In our study, high-order shimming was used in order to circumvent such effects. Furthermore, IRON allows the clear visualization of functional lymph nodes only after contrast agent administration. Therefore, for the differentiation between functional and metastatic lymph nodes, the additional acquisition of precontrast T_1-weighted images will still be necessary. Thus, IRON images are not likely to be a replacement of conventional techniques, but may rather be a useful adjunct.

In conclusion, IRON in concertwith superparamagnetic nanoparticles creates positive signal in normal lymph nodes and can be used to perform ‘positive contrast’ MR-lymphography, in particular, at 3 days after injection of the contrast agent. The potential of this technique to differentiate between normal and metastatic lymph nodes remains to be investigated in future studies.

ACKNOWLEDGMENTS

Dr. Matthias Stuber is compensated as a consultant by Philips Medical Systems, Netherlands, the manufacturer of the equipment described in this presentation. The terms of this agreement have been approved by the Johns Hopkins University in accordance with its conflict of interest policies.

Contract grant sponsor: Donald W. Reynolds Foundation; Contract grant sponsor: National Institutes of Health (NIH); Contract grant numbers: 1 K08 EB004922-01 (to M.S.), R01 HL084186 (to M.S.), R24CA92782 (to R.W.), P50CA86355 (to R.W.).

REFERENCES

1. Weissleder R, Elizondo G, Wittenberg J, Lee AS, Josephson L, Brady TJ. Ultrasmall superparamagnetic iron oxide: an intravenous contrast agent for assessing lymph nodes with MR imaging. Radiology 1990;175:494–498. [PubMed: 2326475]
2. Weissleder R, Heautot JF, Schaffer BK, et al. MR lymphography: study of a high-efficiency lymphotrophic agent. Radiology 1994;191:225–230. [PubMed: 8134576]
3. Vassallo P, Matei C, Heston WD, McLachlan SJ, Koutcher JA, Castellino RA. AMI-227-enhanced MR lymphography: usefulness for differentiating reactive from tumor-bearing lymph nodes. Radiology 1994;193:501–506. [PubMed: 7972768]
4. Choi SH, Han MH, Moon WK, et al. Cervical lymph node metastases: MR imaging of gadofluorine M and monocrystalline iron oxide nanoparticle-47 in a rabbit model of head and neck cancer. Radiology 2006;241:753–762. [PubMed: 17032913]
5. Choi SH, Moon WK, Hong JH, et al. Lymph node metastasis: ultrasmall superparamagnetic iron oxide-enhanced MR imaging versus PET/CT in a rabbit model. Radiology 2007;242:137–143. [PubMed: 17090719]
6. Heesakkers RA, Futterer JJ, Hovels AM, et al. Prostate cancer evaluated with ferumoxtran-10-enhanced T2*-weighted MR imaging at 1.5 and 3.0 T: early experience. Radiology 2006;239:481–487. [PubMed: 16641354]
7. Memarsadeghi M, Riedl CC, Kaneider A, et al. Axillary lymph node metastases in patients with breast carcinomas: assessment with nonenhanced versus USPIO-enhanced MR imaging. Radiology 2006;241:367–377. [PubMed: 17057065]
8. Anzai Y, Piccoli CW, Outwater EK, et al. Evaluation of neck and body metastases to nodes with ferumoxtran 10-enhanced MR imaging: phase III safety and efficacy study. Radiology 2003;228:777–788. [PubMed: 12954896]
9. Harisinghani MG, Barentsz J, Hahn PF, et al. Noninvasive detection of clinically occult lymph-node metastases in prostate cancer. N Engl J Med 2003;348:2491–2499. [PubMed: 12815134]

10. Koh DM, Brown G, Temple L, et al. Rectal cancer: mesorectal lymph nodes at MR imaging with USPIO versus histopathologic findings—initial observations. Radiology 2004;231:91–99. [PubMed: 14976266]
11. Bakker CJ, Seppenwoolde JH, Vincken KL. Dephased MRI. Magn Reson Med 2006;55:92–97. [PubMed: 16342154]
12. Seppenwoolde JH, Viergever MA, Bakker CJ. Passive tracking exploiting local signal conservation: the white marker phenomenon. Magn Reson Med 2003;50:784–790. [PubMed: 14523965]
13. Cunningham CH, Arai T, Yang PC, McConnell MV, Pauly JM, Conolly SM. Positive contrast magnetic resonance imaging of cells labeled with magnetic nanoparticles. Magn Reson Med 2005;53:999–1005. [PubMed: 15844142]
14. Mani V, Briley-Saebo KC, Hyafil F, Fayad ZA. Feasibility of in vivo identification of endogenous ferritin with positive contrast MRI in rabbit carotid crush injury using GRASP. Magn Reson Med 2006;56:1096–1106. [PubMed: 17036302]
15. Mani V, Briley-Saebo KC, Itskovich VV, Samber DD, Fayad ZA. Gradient echo acquisition for superparamagnetic particles with positive contrast (GRASP): sequence characterization in membrane and glass superparamagnetic iron oxide phantoms at 1.5T and 3T. Magn Reson Med 2006;55:126–135. [PubMed: 16342148]
16. Stuber M, Gilson W, Schar M, et al. Positive contrast visualization of iron oxide-labeled stem cells using inversion recovery with ON-resonant water suppression (IRON). Magn Reson Med 2007;58:1072–1077. [PubMed: 17969120]
17. Shen T, Weissleder R, Papisov M, Bogdanov A Jr, Brady TJ. Monocrystalline iron oxide nanocompounds (MION): physicochemical properties. Magn Reson Med 1993;29:599–604. [PubMed: 8505895]
18. Wunderbaldinger P, Josephson L, Weissleder R. Tat peptide directs enhanced clearance and hepatic permeability of magnetic nano-particles. Bioconjug Chem 2002;13:264–268. [PubMed: 11906263]
19. Etienne A, Botnar RM, Van Muiswinkel AM, Boesiger P, Manning WJ, Stuber M. “Soap-Bubble” visualization and quantitative analysis of 3D coronary magnetic resonance angiograms. Magn Reson Med 2002;48:658–666. [PubMed: 12353283]
20. Kraitchman DL, Tatsumi M, Gilson WD, et al. Dynamic imaging of allogeneic mesenchymal stem cells trafficking to myocardial infarction. Circulation 2005;112:1451–1461. [PubMed: 16129797]

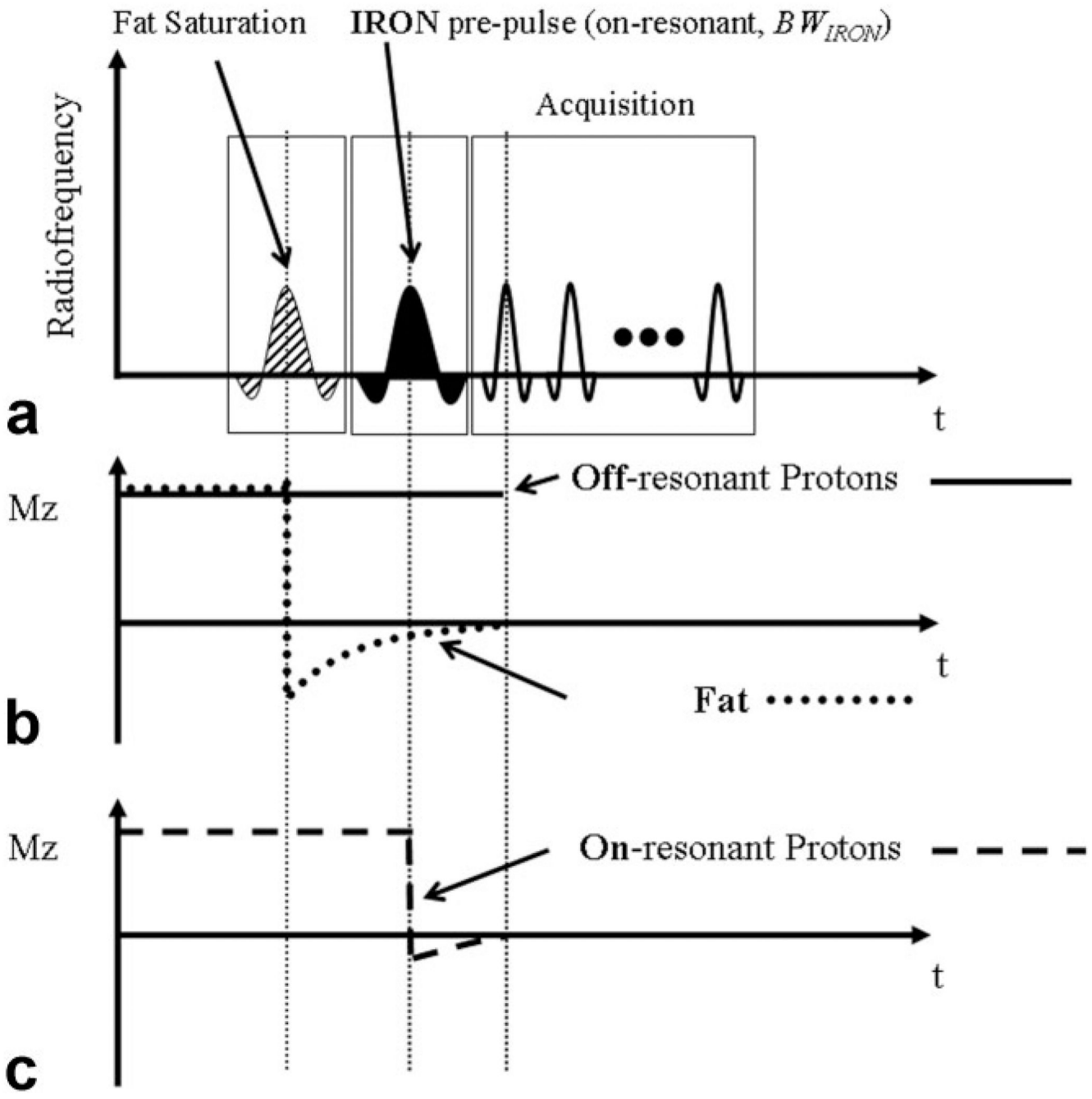

Figure 1.
IRON utilizes a spectrally selective saturation pre-pulse which does not affect off-resonance in close proximity to the superparamagnetic nanoparticles (**a**) and simultaneously suppresses signal originating from on-resonant protons (**b**). Thus, signal enhancement adjacent to these particles can be generated while the on-resonant background and fat appears signal attenuated (**b,c**).

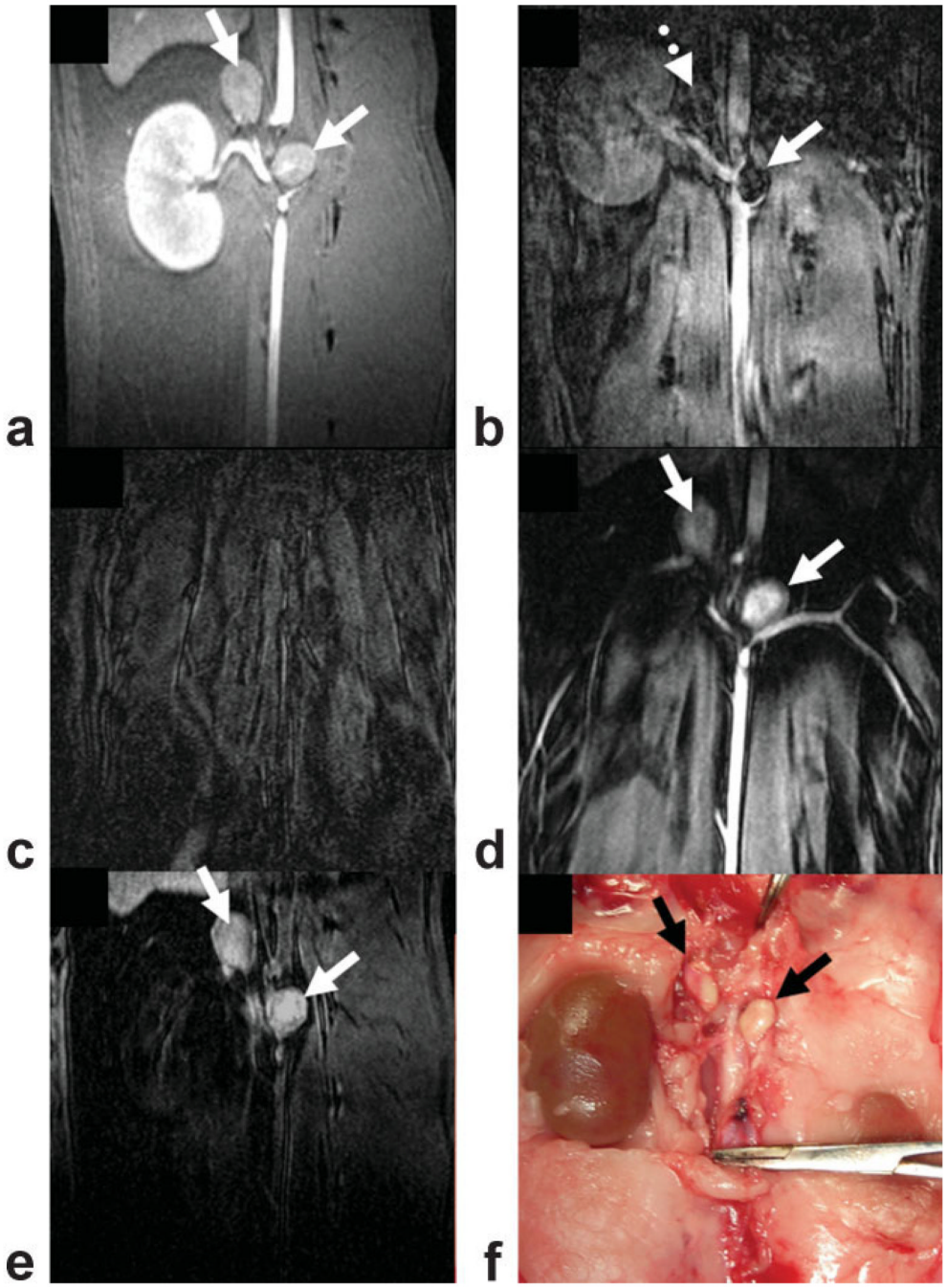

Figure 2.
On coronal T_1-weighted images two paraaortic lymph nodes could be identified at the level of the renal arteries (**a**, solid arrows). After MION-47 administration the lymph nodes showed signal void on T_2*-weighted images (**b**, solid arrow). However, the clear identification of this signal attenuation was often compromised due to general lack of signal in areas of lymph nodes (b, dotted arrow). Using IRON, fat, muscle, and blood were homogeneously suppressed at baseline (**c**). After 24 hours, high contrast enhancement was present both in the aorta and the paraaortic lymph nodes (**d**, solid arrows). After 3 days, contrast enhancement approached baseline in the vessels but persisted in the lymph nodes (**e**, black arrows).

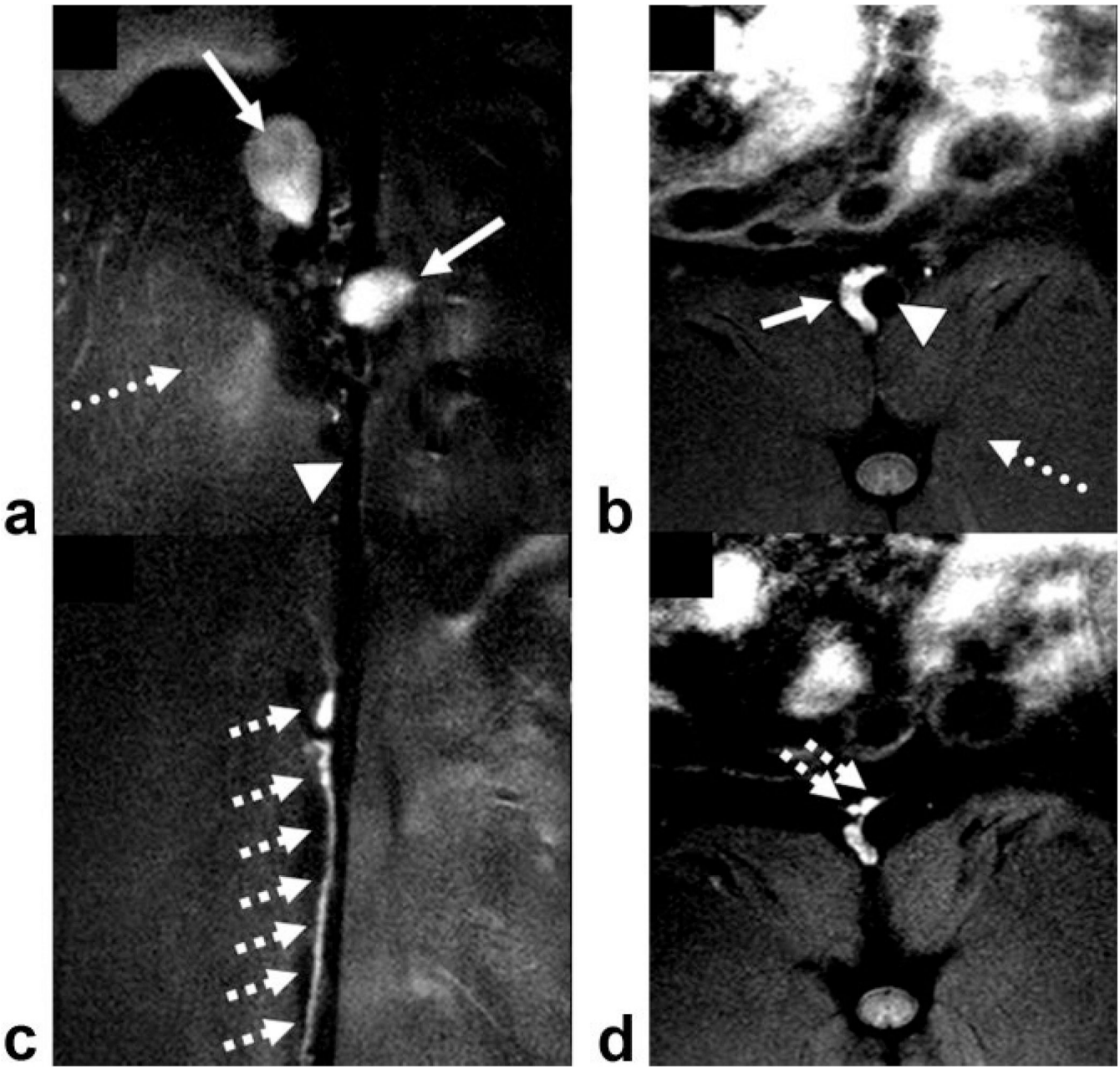

Figure 3.
Postcontrast coronal (**a,c**) and axial (**b,d**) fast spin echo images using IRON demonstrate high contrast enhancement in paraaortic lymph nodes (solid arrows, a,b) and in the paraaortic lymphatic ducts (hatched arrows, c,d), while the abdominal aorta (arrowheads, a,b) and the adjacent muscles are signal attenuated (dotted arrows, a,b).

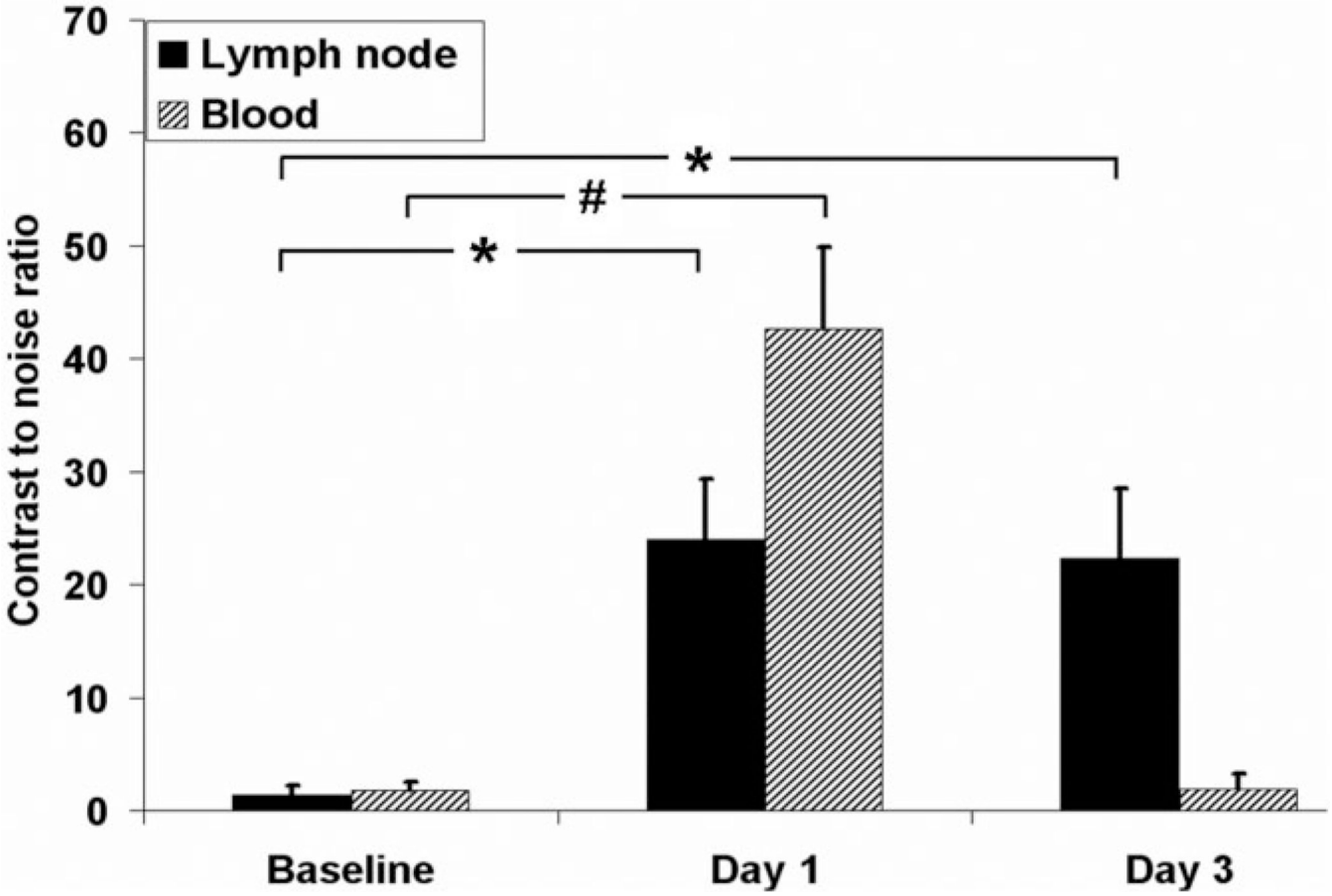

Figure 4.

Quantitative assessment showed that with IRON CNR markedly increased in paraaortic lymph nodes after 24 hours (*P < 0.01 vs. baseline) and remained high up to 3 days after MION-47 injection (*P < 0.01 vs. baseline). In the aorta, CNR was high 24 hours after MION-47 administration (#P < 0.01 vs. baseline) but returned to baseline after 3 days (P = NS vs. baseline).

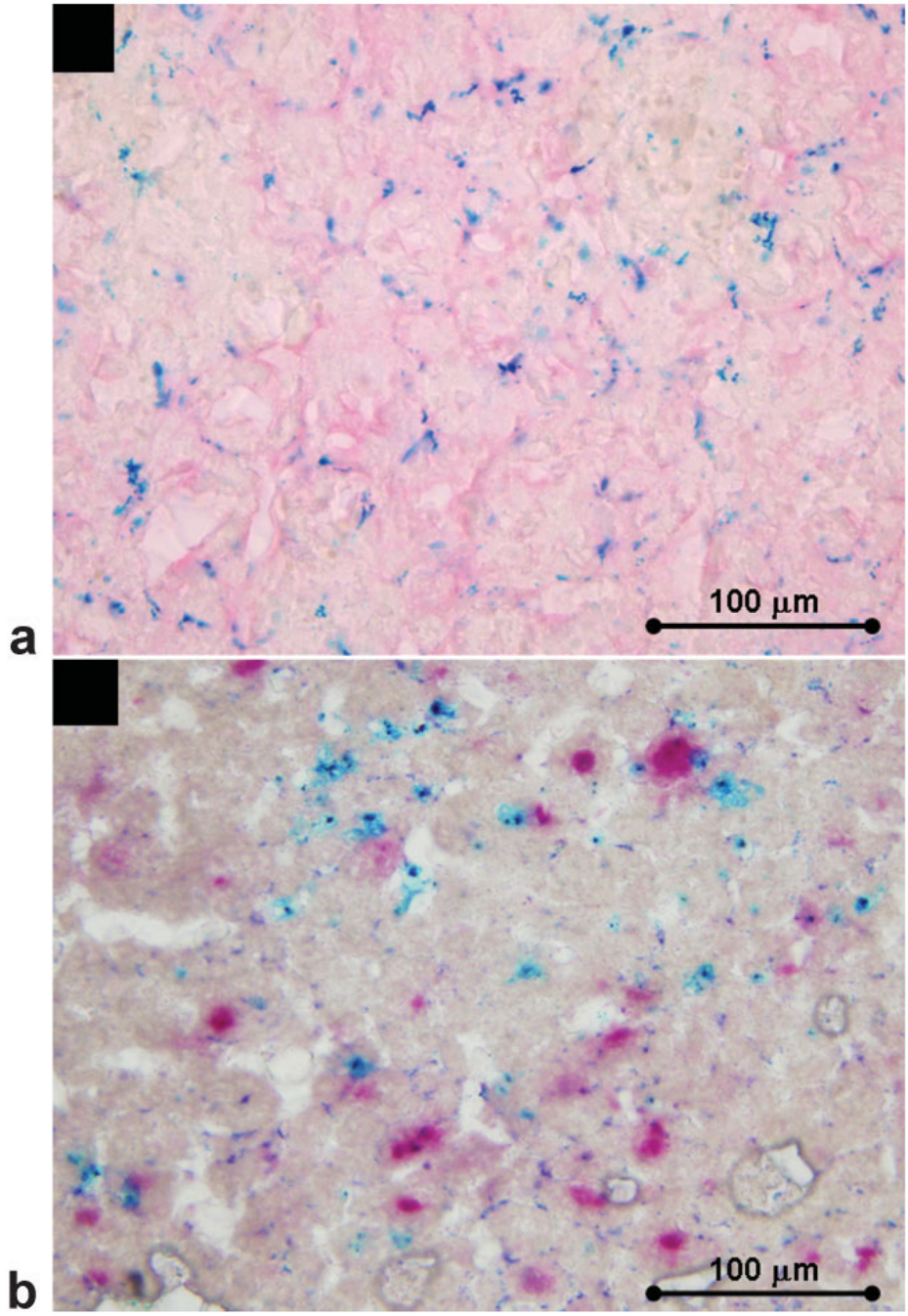

Figure 5.
Prussian blue-positive staining representing iron oxide particles was detected in lymph nodes section counterstained with fast nuclear red (a). Combined acid phosphatase and Prussian blue staining shows colocalization of nodal macrophages and accumulated iron (b).